Fu Lan (Orcid ID: 0000-0002-9070-8373)

RESEARCH ARTICLE

Axial p-n junction design and characterization for InP nanowire array solar cells

Qian Gao[1], Ziyuan Li[1], Li Li[2], Kaushal Vora[2], Zhe Li[3], Ahmed Alabadla[1], Fan Wang[1], Yanan Guo[1], Kun Peng[1], Yesaya C. Wenas[1], Sudha Mokkapati[1], Fouad Karouta[2], Hark Hoe Tan[1], Chennupati Jagadish[1], and Lan Fu[1]

[1]Department of Electronic Materials Engineering, Research School of Physics and Engineering, The Australian National University, Canberra, ACT 2601, Australia
[2]Australian National Fabrication Facility, Research School of Physics and Engineering, The Australian National University, Canberra, ACT 2601, Australia
[3]Department of Applied Mathematics, Research School of Physics and Engineering, The Australia National University, Canberra, ACT 2601, Australia

Correspondence
Lan Fu, Department of Electronic Materials Engineering, Research School of Physics and Engineering, The Australian National University, Canberra, ACT 2601, Australia
Email: lan.fu@anu.edu.au

Abstract

In this work, InP nanowire (NW) array solar cells with different axial p-i-n junction designs were investigated. The optical properties of the different NW structures were characterized through a series of micro-photoluminescence measurements to extract important material parameters such as minority carrier lifetimes and internal quantum efficiencies. A glancing angle sputtering deposition technique has been developed to enable a direct visualization of the p-n junctions in the vertical array of InP NW solar cells (NWSCs) using electron beam induced current (EBIC) technique. Based on EBIC and electrical simulation, it is found that

This is the author manuscript accepted for publication and has undergone full peer review but has not been through the copyediting, typesetting, pagination and proofreading process, which may lead to differences between this version and the Version of Record. Please cite this article as doi: 10.1002/pip.3083

the background doping in NWSC significantly affects the junction position. By modifying the junction design, the width and position of the p-n junction can be varied effectively. By employing a p-p$^-$-n structure, a high junction position (> 1 μm from the substrate) and wide depletion width have been achieved as confirmed by EBIC measurement. Moreover, the NW growth substrate does not show any influence on the device behavior due to the fully de-coupled junction position, indicating a promising structural design for future development of high-performance, low-cost flexible NW devices.

KEYWORDS

III-V compound semiconductors, nanowire array solar cells, axial junction, selective-area MOVPE, EBIC, electroluminescence

1. INTRODUCTION

With their unique structural, optical and electrical properties, III-V semiconductor nanowires (NWs) have shown great potential for novel nanoscale device applications, such as light-emitting diodes (LEDs),[1] lasers,[2-4] photodetectors[5-7] and solar cells.[8-10] In particular, semiconductor NWs are considered to be highly promising for next-generation photovoltaic devices due to: 1) their intrinsic antireflection effect for enhancing light absorption; 2) their small footprint efficiently relaxing the lattice-mismatched strain and thus enabling the construction of multi-junction cells

with optimal band gap combinations as well as the growth on different substrate materials such as silicon and thus potential integration with the existing silicon-based industrial infrastructures;[11,12] and 3) significant cost reduction due to much less material usage.

With a suitable and direct bandgap, superior carrier mobility and well-developed synthesis techniques, significant progress has been made in solar cells fabricated from III-V NW arrays [8,13-19]. Especially for axial p-i-n junction based array NW solar cells (NWSCs), top-down approach led to a record efficiency as high as 17.8%.[20] In terms of bottom-up approach, 15% and 15.3% has been achieved in InP[21] and GaAs[18] array NWSCs respectively by Au-assisted vapor-liquid-solid growth. Up to 6.35% efficiency has also been demonstrated in radial junction InP array NWSCs grown by selective-area metalorganic vapor phase epitaxy (SA-MOVPE),[15,19] however there has been no further report on selective area epitaxy (SAE) grown axial junction InP array NWSCs. Pure wurtzite (WZ) InP NWs with low surface recombination velocity (SRV) (~161 cm/s) has been demonstrated by SA-MOVPE.[3,22] With a careful optimization of junction design (in terms of width and position), growth and device fabrication, it is expected that high performance axial junction InP array NWSCs by SAE can be achieved.

For InP array NWSCs, it has been shown that by varying the length of the bottom p^+-segment[23] and the top n-segment[8] the solar cell performance can be optimized, highlighting the importance of junction position for efficient light absorption and carrier collection in NWSCs. Normally for planar axial junction solar cells, the p-n junction design can be optimized relatively easily through a few growth calibration cycles. However, due to the complex nature of NW growth, background doping, growth rate and dopant diffusion may vary greatly during the growth of different NWSC structures with different p, i, n-segment designs. As a result, the junction position and size may significantly deviate from the original design[24,25] and moreover, the material quality (both optical and electrical) of the NWSC structures may also vary significantly, making it challenging to understand and optimize the NWSC performance. Therefore, it is highly desirable to employ a technique which is able to directly visualize the width and position of the p-n junction for device optimization. Electron beam induced current (EBIC) measurement which uses electron beam to excite the carriers and measure the short circuit current flowing in a material is commonly used to identify junction position and estimate minority carrier diffusion length in planar photovoltaic devices.[26,27] Due to the inherent structural characteristics of NWs such as high aspect ratio, cylindrical shape and difficulties in making electrical contacts, it is challenging to apply EBIC to NW device applications. So far

there have been a few reports on EBIC measurements of p-n junction of single NWs,[21,25,28-30] however very little has been reported on EBIC of NWs in vertical array configuration[31-33] where additional information could be obtained such as identifying the possible substrate influence on NWSCs as well as evaluating the uniformity of electrical performance of a large number of NWs. In this paper, we demonstrate for the first time direct junction characterization and analysis of SAE-grown axial junction InP NW array solar cells based on EBIC measurements and electrical simulation.

It is well known that due to background impurity doping, the unintentionally doped InP grown by MOVPE is normally n-type.[34] We also found that the InP NWs grown by the SAE technique exhibit a relatively high background doping density[24] of ~10^{17} cm^{-3}, which has to be taken into consideration when designing p-n junction for solar cell applications. In this work three different InP NWSC structures grown on p-doped InP substrate by SA-MOPE, namely i(n^-)-n, p-i(n^-)-n and p-p^--n, were designed and characterized using EBIC technique. We show that compared with the other two structures, by introducing a lightly p-doped middle segment, the depletion region in the p-p^--n structure can be successfully shifted closer to the top of the NWs which is more favorable for light absorption and carrier separation.[8] More importantly, it is also revealed that in the p-p^--n structure the influence from the NW growth substrate has been completely eliminated, allowing the assessment of the true performance of the

NW array solar cell devices. This structure also presents the most suitable device design for future development of flexible NW devices by detaching them from the substrate using flexible polymer materials and reusing the substrate to reduce cost. Despite a slightly reduced carrier lifetime and internal quantum efficiency (IQE) in the junction (depletion) region due to p-dopant incorporation as indicated by time-resolved photoluminescence (TRPL) measurements, a good efficiency of up to 9.23% has been obtained from the p-p^--n structure without any surface passivation. Our results emphasize the importance of a comprehensive electrical structure and material design, providing a good guidance for development of future high-efficiency, low-cost, flexible NWSC devices.

2. EXPERIMENTAL DETAILS

To grow the InP NW arrays, p^+ (111)A InP substrates were firstly deposited with a 30 nm-SiO_x layer by plasma enhanced chemical vapor deposition and then patterned by electron beam lithography. Wet chemical etching was used to open up holes followed by InP NW growth in a horizontal low pressure (100 mbar) MOVPE system (Aixtron 200/4) at the growth temperature of 730 ºC. Trimethylindium (TMIn) and phosphine (PH_3) were used as precursors for the group III (In) and group V (P) elements, respectively. Flow rates were set at 6.1×10^{-6} and 4.9×10^{-4} mol/min, respectively for

TMIn and PH_3, corresponding to a V/III ratio of 80. For n-doped segment, silane was introduced during the growth at flow rate of 3.1×10^{-7} mol/min with all other parameters kept constant. Diethylzinc was used as p-dopant,[35] and the flow rate of 2.5×10^{-7} and 2.0×10^{-5} mol/min were used for p^- and p-doped segment, respectively.

For PL and time-resolved PL measurements, the NWs were excited using a 522 nm (frequency doubled) pulsed laser source with pulse width of 300 fs and repetition rate of 20.8 MHz. The laser beam was focused using a 100 × (NA 0.75) microscope objective lens on the middle of the NWs, with a spot size of 0.72 μm estimated by vector diffraction calculation.[36]. The emission was detected by a single photon avalanche diode, which was connected to the time-correlated single photon counting (TCSPC) system (Picoharp 300). The minority carrier lifetime was extracted from a single or double exponential fitting of time-resolved photoluminescence (TRPL) decay curve measured by the TCSPC system.

For EBIC measurements, an indium tin oxide (ITO) layer was deposited on top of the NW array by glancing angle sputter coating to obtain a complete coverage of ITO only on the tip of the NWs (n-region) to enable good electrical connection. This method has been developed to avoid the planarization of the NW array. EBIC measurement was carried out in a FEI Helios 600 Nanolab dual beam FIB system equipped with Kleindiek NanoControl NC40 nano-manipulators and low current

measurement units. The top electrode and bottom electrode of the sample were contacted to the nanomanipulator and sample stage respectively, allowing electrical current to flow and pass through a current amplifier.

3. RESULTS AND DISCUSSION

3.1. Photoluminescence and time-resolved photoluminescence

The InP NW array design has been optimized by the finite-difference time-domain (FDTD) simulation to achieve maximum light absorption with 200 nm-diameter NWs arranged in a hexagonal array with 400 nm spacing.[37] Three InP NWSC samples with the same array parameters but different structural designs have been grown on p^+ InP substrates and illustrated schematically in Figure 1A. Sample I (i-n^+) was grown with an undoped section for 7 min on the p^+ substrate followed by a heavily n-doped section for 2 min. Sample II (p-i-n^+) shows the InP NW array with a p-doped section (1.5 min) firstly grown on the p^+ substrate followed by an undoped section (5 min) and a heavily n-doped section (1.5 min). Sample III (p-p^--n^+) was grown with a p-doped section (1.5 min) on the p^+ substrate followed by a lightly p-doped section (5 min) and a heavily n-doped section (1.5 min). The doping concentrations of both n-doped and undoped sections were calibrated based on our previous doping study.[24] However

despite a high doping concentration aimed for the bottom p-region for samples II and III, we find it difficult to determine the p-type doping concentration using both the photoluminescence (PL) and electrical measurements which were previously used to determine the n-type doping concentration with great success,[24] implying that the p-region of our NWs may be only lightly doped ($< 1\times10^{17}$ cm^{-3}) despite that a high diethylzinc (DEZn) flow rate was used. This may be due to the relatively high growth temperature of 730 ºC used for the NW growth which is known to be unfavourable for incorporation of Zn-dopant by MOVPE. Figure 1B shows the scanning electron microscopy (SEM) image of the NW array taken from Sample I. The typical diameter of the NWs is ~200 nm and the average length of the NWs is ~1.4, 1.5, 1.8 μm for Samples I, II, III, respectively. The different NW length is mainly due to the slight variation of the device structural design as well as the different doping conditions that could largely affect the NW growth rate. High resolution transmission electron microscopy (TEM) examination along the length of the NW shows that even with different types and levels of doping, all three samples are pure WZ phase (See Figure S1, Supporting Information).

After growth, some NWs were mechanically transferred from the array to a SiN_x coated Si substrate for micro-PL and TRPL measurements, to allow direct probing of the middle segment of the NWSC structure. More than ten NWs were measured for

each sample. Figure 2A shows the typical room-temperature single NW PL spectra from the three NWSC samples. All spectra feature a main peak with a shoulder at higher energy, which can be fitted with two Gaussian peaks at the energy of 1.42 and 1.44 eV, respectively (See Figure S2, Supporting Information). We attribute the lower energy peak to the band edge emission (A band) from WZ InP NWs and the higher energy peak to the split off valence band (B band).[38,39] The PL spectra are normalized to the peak intensity of Sample I NW. It can be seen that Sample I exhibits the highest PL peak intensity and Sample III shows the lowest PL peak intensity. The full width at half-maximum (FWHM) of Samples I, II and III are 32, 41 and 47 nm, respectively.

The room-temperature minority carrier lifetimes are also extracted from the three different NW samples by fitting their TRPL spectral decays. For Samples I and II, the TRPL decay can be fitted well with mono-exponential decay, as shown in Figure 2B, with minority carrier lifetimes of 1.64 and 1.37 ns, respectively. For Sample III, an initial sharp decay followed by one with much slower decay rate has been observed. The sharp decay may be attributed to a rapid field-assisted trapping of photon-injected minority electrons at the surface of NWs,[40] while the slower decay is dominated by the minority carrier lifetime of the p-doped NW. Hence for Sample III, the spectrum is fitted with double exponential decays and a minority carrier lifetime of ~1.22 ns is obtained from the slow decay portion of the curve. Again compared with Sample I, the

minority carrier lifetimes in Samples II and III are found to be reduced. Finally, as a quantitative estimation of the material optical quality, the IQE for NWs from Samples I, II and III were measured based on the method described by Fan *et al.*[24] (See Figure S3, Supporting Information). From Figure 2C, the highest IQE has been obtained for Sample I (~58%) followed by ~37% for Sample II and ~26% for Sample III.

As suggested from the above PL (intensity/FWHM), minority carrier lifetimes and IQE results, Sample I shows the best optical quality, followed by Sample II and Sample III. It is well-known that the PL properties of semiconductor materials strongly depend on the growth conditions (methods and parameters), doping concentrations, and impurity species. We ascribe the degraded optical properties in Sample II and Sample III to the effect of Zn diffusion and/or doping, which is a well-recognized problem for InP growth by MOVPE, especially at high growth temperatures.[19] Since both Samples II and III were grown with an intentionally p-doped segment first at a relatively high DEZn flow rate (2.0×10^{-5} mol/min) and growth temperature (730 °C), Zn could outdiffuse from the p-segment and/or due to the "memory effect" in the reactor to incorporate into the middle undoped (Sample II) or lightly p^--doped (Sample III) segment during its growth. Indeed, it has been found from studies of p-doped InP layers by thermal diffusion[41] that Zn diffusion proceeds via an interstitial-substitutional kick-out mechanism[42-45] and consequently leads to a high

concentration of interstitial Zn atoms. Similarly during the MOVPE growth of Samples II and III, Zn incorporation into the middle segment of the NWSC structure may likely form some Zn interstitials in addition to achieving of a low p-doping concentration. Zn interstitials have been identified as the main reason causing a degraded PL in Zn-doped InP NWs.[46] P-doping could also lead to broadening of the FWHM of the PL spectrum due to the impurity band that merges with the valence band edge as band tail states and thus broaden optical transitions between the conduction and valence bands.[47] Furthermore, it is well known that doping may cause reduced carrier lifetime and mobility as a result of ionized impurity scattering.[48,49] Therefore, compared with Sample I, increasingly degraded PL intensity, FWHM and carrier lifetime are observed from Samples II and III.

3.2. EBIC measurements

EBIC measurements provide a direct visualization of the p-n junctions in the three NWSC structures. Our EBIC measurements were performed under an SEM column at 1 kV with a beam current of ~86 pA. The maximum penetration depth of electrons in the sample is calculated to be ~30 nm at 1 kV using the Casino simulation software (See Figure S4, Supporting Information). During the measurements, the NW samples were unbiased, such that the EBIC signal is solely due to the separation of the electron

beam generated nonequilibrium carriers by the built-in field of the junction and the diffusion of minority carriers from each side of the p-n junction reaching the field. Figure 3 shows the SEM images (the first column) and their corresponding EBIC images (the second column) taken from Samples I, II and III, in comparison with the electric field distribution profiles determined by Comsol Multiphysics simulations (See Supporting Information Section 3.2) of their respective p-i-n structure designs. The relative EBIC intensity is presented by the red curve along the center of the NW as obtained from ImageJ Processing Software. As mentioned earlier, based on our previous study[24] undoped InP NWs are normally n-type with a doping concentration of ~1×10^{17} cm^{-3}. Therefore, from the EBIC image which shows a number of NWs of Sample I (Figure 3B), consistently bright contrasts can be observed at all NW/substrate interfaces, which is a clear indication of the built-in electric field formed between the undoped (n-type) segment and p-type substrate. Weaker EBIC signal contrasts can also be observed above the bright regions in the NWs due to the minority carrier diffusion. Electrical modelling was performed to estimate the electric field distribution in the NWSC based on a doping profile of highly doped p^+ substrate (5×10^{18} cm^{-3})-i (n^- ~10^{17} cm^{-3})-n^+ (3×10^{18} cm^{-3}) with the doping concentrations calibrated by our previous work.[24] The result shown in Figure 3C clearly indicates the formation of the electric field within the NW (as a result of high p^+ doping in substrate

and lower n background doping in the NW) with a depletion width of ~135 nm in the NW from the NW/substrate interface which is consistent with EBIC results.

The SEM image of Sample II and its corresponding EBIC image are shown in Figure 3D and Figure 3E, respectively. As displayed in Figure 3E, a bright contrast can be observed in the middle of the NW. It is clearly found the built-in electric field region is formed between the undoped segment and bottom p-type segment, and the undoped segment is slightly n-type despite that possible Zn diffusion may also have occurred during its growth. Above and below the bright depletion region, slightly weaker EBIC signals are also obtained, which can be again ascribed to minority carrier diffusion currents, i.e., arising from the electron beam generated electrons and holes that diffuse towards the depletion region of this sample. The simulation results in Figure 3F show the formation of an electric field region with an estimated depletion width of ~110 nm in the NW (based on a p (~5×10^{16} cm^{-3})-i (n^- ~1×10^{17} cm^{-3})- n^+ (3×10^{18} cm^{-3}) junction), which agrees well with the EBIC results.

By lightly p-doping the middle segment, Sample III has a depletion region which is the closest to the top of the NWs as evidenced by the bright contrast of the EBIC signal shown in Figure 3H. There are also two regions with less signal intensity being observed from each side of the junction, which can again be attributed to the electron beam induced minority carrier diffusion. Based on a doping profile of p (5×10^{16}

cm^{-3})-i (p^- ~1×10^{16} cm^{-3})-n^+ (3×10^{18} cm^{-3}), a depletion width of ~300 nm in the NW (across the p^-/n^+ interface) is estimated from the electrical simulation (shown in Figure 3I), which is consistent with the EBIC measurement shown in Figure 3H. The EBIC results suggest that among the three NWSC structures the most promising junction design is that of Sample III, where a longer depletion region has been produced closer to the top of the NW (just below the n^+ segment) to enable an effective light absorption and carrier separation.

Minority carrier diffusion length is an important parameter indicating carrier collection probability of solar cells. It has been found that surface recombination plays an important role on carrier diffusion length in both Si[50] and III-V NWs. For example, GaAs NWs have been reported with very short carrier diffusion lengths (< 100 nm) compared with surface passivated GaAs NWs with AlGaAs shell (~1000 nm)[51] due to the high SRV of GaAs. Similarly, GaN/AlGaN core-shell NWs have been reported with long carrier diffusion length for holes (L_p, 1200 nm) whereas that of the uncapped GaN NWs is significantly shorter (130 - 710 nm).[52,53] Based on the EBIC results from Figure 3, carrier diffusion lengths for electrons (L_n) and holes (L_p) were extracted by exponentially fitting the EBIC signal as a function of the illumination position along the NW.[29] As shown in Figure 4, a hole diffusion length L_p of 553 and 193 nm were extracted from the undoped i-side (n^-) for Samples I and II respectively. The longer L_p

on the undoped i-side (n^-) of Sample I compared to Sample II corresponds well with the PL and minority carrier lifetime results, indicating the influence of Zn diffusion. An electron diffusion length (L_n) was extracted to be 228 nm on the p^--side for Sample III. Compared with previously reported p-n InP NWs which have L_n and L_p of 160 and 65 nm (with the doping concentration for p-doped and n-doped segments of 5×10^{18} and 1×10^{19} cm^{-3}, respectively),[28] the longer L_n and L_p obtained from our NWSC structures may be due to the much lower doping concentration as well as the defect-free pure WZ crystal phase of the NWs.

As clearly indicated from the EBIC measurements, since both Samples I and II have low junction positions, minority carriers generated from the substrate could diffuse to the junction to contribute to the photocurrent making it hard to differentiate the contribution from the NW and the substrate; whereas in Sample III (p-p^--n structure) due to its higher junction position (> 1 μm from the substrate) and limited carrier diffusion length, we may exclude the possibility of photocurrent generation from the substrate. This will allow us to assess the real device performance of the NWSC array, which is critical for enabling their future applications as flexible/wearable devices where the NW array needs to be detached (or peeled off) from the substrate.[54,55]

3.3. Solar cell performance

An n-p$^-$-p sample (the same as Sample III) containing six 200 μm by 200 μm NW arrays was grown and fabricated into solar cell devices through photoresist (AZ 5214E) planarization, oxygen plasma etching to uncover the NW tips, transparent contact ITO deposition (~500 nm) using sputtering technique and Ti/Au contact deposition (10 nm/200 nm) using electron-beam evaporation. Figure 5A shows the schematic diagram of the device structure. The solar cell performance was characterized by current-voltage (I-V) measurements under dark and light (1 sun AM 1.5G) conditions, the results of which are shown in Figure 5B. From the J-V results, an open-circuit voltage of 0.55 V, a short-circuit current density of 22.5 mA/cm^2, and a fill factor of 0.75 were obtained, leading to an overall conversion efficiency of ~9.23%. It should be noted that during the device fabrication process, no chemical treatment [56] and/or oxide surface passivation[8,20,21] was performed. It is expected that with a further optimization of surface passivation, the device performance can be significantly improved. Figure 5C presents the room-temperature electroluminescence (EL) spectrum of the solar cell device measured at 2.59 mA, displaying a strong EL peak at 1.42 eV. This corresponds to the bandgap of pure WZ InP NW[57,58] and again confirms that the depletion region in the n-p$^-$-p sample is de-coupled from the zinc blende (ZB) InP substrate such that no substrate related EL peak[23] is observed. Based on our work, it is believed that by further optimization of the p-p$^-$-n NWSC structural

design and growth based on EBIC measurement and device simulation (e.g., significant reduction of the length of the top n-segment,[8] fine tuning of the doping and length of p and p^- segments) as well as device fabrication (implementation of surface passivation), large improvement in device performance can be achieved in our SAE grown axial junction InP NWSCs.

4. CONCLUSION

In conclusion, EBIC measurements combined with electrical simulation and optical characterization have been carried out to characterize three InP NWSC samples with different axial p-i-n junction designs. It is shown that by varying the doping profile of the solar cell structures, the junction position and width can be adjusted and placed towards the top of the NWs by employing a p-p^--n structure, where more efficient light absorption and carrier collection can be achieved. With the junction positioned away from the NW growth substrate, the parasitic photocurrent generation from the substrate was also effectively eliminated. This will allow us to evaluate the true performance of the NW array solar cells without any influence from the NW growth substrate. Moreover, this structural design can also be used as a suitable device platform for fabricating flexible/wearable devices in the future by detaching the NW array from the substrate and at the same time enabling a re-usable substrate for

repeated NW growth to significantly reduce material cost. Despite slightly degraded optical properties of the NWs due to Zn-diffusion and/or doping, up to 9.23% solar cell efficiency has been achieved in the p-p$^-$-n NW arrays without any surface passivation. Our study provides important insights into the key issues of material growth and junction design critical for the development of next generation high-performance, low-cost, flexible NW solar cells. The understanding gained from this work can also be further extended to a wide range of nanowire or other novel low dimensional material (such as the emerging 2D materials) based optoelectronic devices including LEDs, lasers, and photodetectors for numerous future applications.

SUPPORTING INFORMATION

Supporting Information (transmission electron microscopy, optical properties, and simulation) is available from the Wiley Online Library or from the author.

ACKNOWLEDGMENTS

The Australian Research Council is acknowledged for financial support. Access to facilities used in this work is made possible through the Australian National Fabrication Facility and Australian Microscopy and Microanalysis Research Facility.

REFERENCES

[1] Minot ED, Kelkensberg F, van Kouwen M, van Dam JA, Kouwenhoven LP, Zwiller V, et al. Single Quantum Dot Nanowire LEDs. Nano Lett 2007;7:367-71.
[2] Saxena D, Mokkapati S, Parkinson P, Jiang N, Gao Q, Tan HH, et al. Optically pumped room-temperature GaAs nanowire lasers. Nat Photonics 2013;7:963-8.
[3] Gao Q, Saxena D, Wang F, Fu L, Mokkapati S, Guo Y, et al. Selective-Area Epitaxy of Pure Wurtzite InP Nanowires: High Quantum Efficiency and Room-Temperature Lasing. Nano Lett 2014;14:5206-11.
[4] Saxena D, Wang F, Gao Q, Mokkapati S, Tan HH, Jagadish C. Mode Profiling of Semiconductor Nanowire Lasers. Nano Lett 2015;15:5342-8.
[5] Peng K, Parkinson P, Fu L, Gao Q, Jiang N, Guo Y-N, et al. Single Nanowire Photoconductive Terahertz Detectors. Nano Lett 2015;15:206-10.
[6] Peng K, Parkinson P, Boland JL, Gao Q, Wenas YC, Davies CL, et al. Broadband Phase-Sensitive Single InP Nanowire Photoconductive Terahertz Detectors. Nano Lett 2016;16:4925-31.
[7] Zhang H, Guan N, Piazza V, Kapoor A, Bougerol C, Julien F, et al. Comprehensive analyses of core–shell InGaN/GaN single nanowire photodiodes. J Phys D Appl Phys 2017;50:484001.
[8] Wallentin J, Anttu N, Asoli D, Huffman M, Åberg I, Magnusson MH, et al. InP Nanowire Array Solar Cells Achieving 13.8% Efficiency by Exceeding the Ray Optics Limit. Science 2013;339:1057-60.
[9] Krogstrup P, Jørgensen HI, Heiss M, Demichel O, Holm JV, Aagesen M, et al. Single-nanowire solar cells beyond the Shockley–Queisser limit. Nat Photonics 2013;7:306-10.
[10] Cui Y, van Dam D, Mann SA, van Hoof N, van Veldhoven P, Garnett E, et al. Boosting Solar Cell Photovoltage via Nanophotonic Engineering. Nano Lett 2016;16:6467-71.
[11] Tomioka K, Motohisa J, Hara S, Fukui T. Control of InAs Nanowire Growth Directions on Si. Nano Lett 2008;8:3475-80.
[12] Tomioka K, Kobayashi Y, Motohisa J, Hara S, Fukui T. Selective-area growth of vertically aligned GaAs and GaAs/AlGaAs core-shell nanowires on Si(111) substrate. Nanotechnology 2009;20:145302.
[13] Yao M, Huang N, Cong S, Chi C-Y, Seyedi MA, Lin Y-T, et al. GaAs Nanowire Array Solar Cells with Axial p–i–n Junctions. Nano Lett 2014;14:3293-303.
[14] Cui Y, Wang J, Plissard SR, Cavalli A, Vu TTT, van Veldhoven RPJ, et al. Efficiency Enhancement of InP Nanowire Solar Cells by Surface Cleaning. Nano Lett 2013;13:4113-7.
[15] Yoshimura M, Nakai E, Tomioka K, Fukui T. Indium Phosphide Core-Shell Nanowire Array Solar Cells with Lattice-Mismatched Window Layer. Appl Phys Express 2013;6:052301.
[16] Mariani G, Scofield AC, Hung C-H, Huffaker DL. GaAs nanopillar-array solar cells employing in situ surface passivation. Nat Commun 2013;4:1497.

[17] Heurlin M, Wickert P, Fält S, Borgström MT, Deppert K, Samuelson L, et al. Axial InP Nanowire Tandem Junction Grown on a Silicon Substrate. Nano Lett 2011;11:2028-31.
[18] Åberg I, Vescovi G, Asoli D, Naseem U, Gilboy JP, Sundvall C, et al. A GaAs Nanowire Array Solar Cell With 15.3% Efficiency at 1 Sun. IEEE J Photovolt 2016;6:185-90.
[19] Goto H, Nosaki K, Tomioka K, Hara S, Hiruma K, Motohisa J, et al. Growth of Core–Shell InP Nanowires for Photovoltaic Application by Selective-Area Metal Organic Vapor Phase Epitaxy. Appl Phys Express 2009;2:035004.
[20] van Dam D, van Hoof NJ, Cui Y, van Veldhoven PJ, Bakkers EP, Gómez Rivas J, et al. High-efficiency nanowire solar cells with omnidirectionally enhanced absorption due to self-aligned Indium-Tin-Oxide Mie scatterers. ACS Nano 2016;10:11414-9.
[21] Otnes G, Barrigón E, Sundvall C, Svensson KE, Heurlin M, Siefer G, et al. Understanding InP Nanowire Array Solar Cell Performance by Nanoprobe-Enabled Single Nanowire Measurements. Nano Lett 2018;18:3038-46.
[22] Gao Q, Dubrovskii VG, Caroff P, Wong-Leung J, Li L, Guo Y, et al. Simultaneous Selective-Area and Vapor-Liquid-Solid Growth of InP Nanowire Arrays. Nano Lett 2016;16:4361-7.
[23] Jain V, Nowzari A, Wallentin J, Borgström M, Messing M, Asoli D, et al. Study of photocurrent generation in InP nanowire-based p+-i-n+ photodetectors. Nano Res 2014;7:544-52.
[24] Wang F, Gao Q, Peng K, Li Z, Li Z, Guo Y, et al. Spatially Resolved Doping Concentration and Nonradiative Lifetime Profiles in Single Si-Doped InP Nanowires Using Photoluminescence Mapping. Nano Lett 2015;15:3017-23.
[25] Zhong Z, Li Z, Gao Q, Li Z, Peng K, Li L, et al. Efficiency enhancement of axial junction InP single nanowire solar cells by dielectric coating. Nano Energy 2016;28:106-14.
[26] Edwards PR, Galloway SA, Durose K. EBIC and luminescence mapping of CdTe/CdS solar cells. Thin Solid Films 2000;372:284-91.
[27] Stolt L, Hedström J, Kessler J, Ruckh M, Velthaus KO, Schock HW. ZnO/CdS/CuInSe2 thin-film solar cells with improved performance. Appl Phys Lett 1993;62:597-9.
[28] Wallentin J, Wickert P, Ek M, Gustafsson A, Wallenberg LR, Magnusson MH, et al. Degenerate p-doping of InP nanowires for large area tunnel diodes. Appl Phys Lett 2011;99:253105.
[29] Gutsche C, Niepelt R, Gnauck M, Lysov A, Prost W, Ronning C, et al. Direct Determination of Minority Carrier Diffusion Lengths at Axial GaAs Nanowire p–n Junctions. Nano Lett 2012;12:1453-8.
[30] Li Z, Yang I, Li L, Gao Q, Chong JS, Li Z, et al. Reducing Zn diffusion in single axial junction InP nanowire solar cells for improved performance. Prog Nat Sci: Mater Int 2018;28:178-82.

[31] Arstila K, Hantschel T, Schulze A, Vandooren A, Verhulst AS, Rooyackers R, et al. Nanoprober-based EBIC measurements for nanowire transistor structures. Microelectronic Engineering 2013;105:99-102.
[32] Tchoulfian P, Donatini F, Levy F, Dussaigne A, Ferret P, Pernot J. Direct Imaging of p–n Junction in Core–Shell GaN Wires. Nano Lett 2014;14:3491-8.
[33] Tchernycheva M, Neplokh V, Zhang H, Lavenus P, Rigutti L, Bayle F, et al. Core–shell InGaN/GaN nanowire light emitting diodes analyzed by electron beam induced current microscopy and cathodoluminescence mapping. Nanoscale 2015;7:11692-701.
[34] Takeda Y, Araki S, Noda S, Sasaki A. Characterization of InP Grown by OMVPE Using Tertiary-butylphosphine for the Phosphorous Source. Jpn J Appl Phys 1990;29:11.
[35] Wallentin J, Borgström MT. Doping of semiconductor nanowires. J Mater Res 2011;26:2142-56.
[36] Török P, Varga P, Laczik Z, Booker GR. Electromagnetic diffraction of light focused through a planar interface between materials of mismatched refractive indices: an integral representation. J Opt Soc Am A 1995;12:325-32.
[37] Li Z, Wenas YC, Fu L, Mokkapati S, Tan HH, Jagadish C. Influence of Electrical Design on Core-Shell GaAs Nanowire Array Solar Cells. IEEE J Photovolt 2015;5:854-64.
[38] Tuin G, Borgström M, Trägårdh J, Ek M, Wallenberg LR, Samuelson L, et al. Valence band splitting in wurtzite InP nanowires observed by photoluminescence and photoluminescence excitation spectroscopy. Nano Res 2011;4:159-63.
[39] De A, Pryor CE. Predicted band structures of III-V semiconductors in the wurtzite phase. Physical Review B 2010;81:155210.
[40] Boland JL, Casadei A, Tu□tu□ncu□oglu G, Matteini F, Davies CL, Jabeen F, et al. Increased Photoconductivity Lifetime in GaAs Nanowires by Controlled n-Type and p-Type Doping. ACS Nano 2016;10:4219-27.
[41] Moon Y, Si S, Yoon E, Kim SJ. Low temperature photoluminescence characteristics of Zn-doped InP grown by metalorganic chemical vapor deposition. J Appl Phys 1998;83:2261-5.
[42] Ky NH, Pavesi L, Araújo D, Ganière JD, Reinhart FK. A model for the Zn diffusion in GaAs by a photoluminescence study. J Appl Phys 1991;69:7585-93.
[43] Ky NH, Ganière JD, Gailhanou M, Blanchard B, Pavesi L, Burri G, et al. Self-interstitial mechanism for Zn diffusion-induced disordering of GaAs/AlxGa1−xAs (x=0.1−1) multiple-quantum-well structures. J Appl Phys 1993;73:3769-81.
[44] Hsu JK, Juang C, Lee BJ, Chi GC. Photoluminescence studies of interstitial Zn in InP due to rapid thermal annealing. J Vac Sci Technol B 1994;12:1416-8.
[45] Montie EA, van Gurp GJ. Photoluminescence of Zn-diffused and annealed InP. J Appl Phys 1989;66:5549-53.
[46] Thuy VTT. Nanowire Photoluminescence for Photovoltaics: Eindhoven University of Technology; 2015.

[47] Hudait MK, Modak P, Rao KSRK, Krupanidhi SB. Low temperature photoluminescence properties of Zn-doped GaAs. Mater Sci Eng: B 1998;57:62-70.
[48] Agashe C, Kluth O, Hüpkes J, Zastrow U, Rech B, Wuttig M. Efforts to improve carrier mobility in radio frequency sputtered aluminum doped zinc oxide films. J Appl Phys 2004;95:1911-7.
[49] Friedland KJ, Hey R, Kostial H, Klann R, Ploog K. New Concept for the Reduction of Impurity Scattering in Remotely Doped GaAs Quantum Wells. Phys Rev Lett 1996;77:4616-9.
[50] Allen JE, Hemesath ER, Perea DE, Lensch-Falk JL, Li ZY, Yin F, et al. High-resolution detection of Au catalyst atoms in Si nanowires. Nat Nanotechnol 2008;3:168-73.
[51] Bolinsson J, Mergenthaler K, Samuelson L, Gustafsson A. Diffusion length measurements in axial and radial heterostructured nanowires using cathodoluminescence. J Cryst Growth 2011;315:138-42.
[52] Baird L, Ang GH, Low CH, Haegel NM, Talin AA, Li Q, et al. Imaging minority carrier diffusion in GaN nanowires using near field optical microscopy. Physica B: Condensed Matter 2009;404:4933-6.
[53] Baird L, Ong CP, Cole RA, Haegel NM, Talin AA, Li Q, et al. Transport imaging for contact-free measurements of minority carrier diffusion in GaN, GaN/AlGaN, and GaN/InGaN core-shell nanowires. Appl Phys Lett 2011;98:132104.
[54] Dai X, Messanvi A, Zhang H, Durand C, Eymery J, Bougerol C, et al. Flexible Light-Emitting Diodes Based on Vertical Nitride Nanowires. Nano Lett 2015;15:6958-64.
[55] Zhang H, Dai X, Guan N, Messanvi A, Neplokh V, Piazza V, et al. Flexible photodiodes based on nitride core/shell p–n junction nanowires. ACS Appl Mater Interfaces 2016;8:26198-206.
[56] Mariani G, Wong P-S, Katzenmeyer AM, Léonard F, Shapiro J, Huffaker DL. Patterned radial GaAs nanopillar solar cells. Nano Lett 2011;11:2490-4.
[57] Mishra A, Titova LV, Hoang TB, Jackson HE, Smith LM, Yarrison-Rice JM, et al. Appl Phys Lett 2007;91:263104.
[58] Pemasiri K, Montazeri M, Gass R, Smith LM, Jackson HE, Yarrison-Rice J, et al. Carrier Dynamics and Quantum Confinement in type II ZB-WZ InP Nanowire Homostructures. Nano Lett 2009;9:648-54.

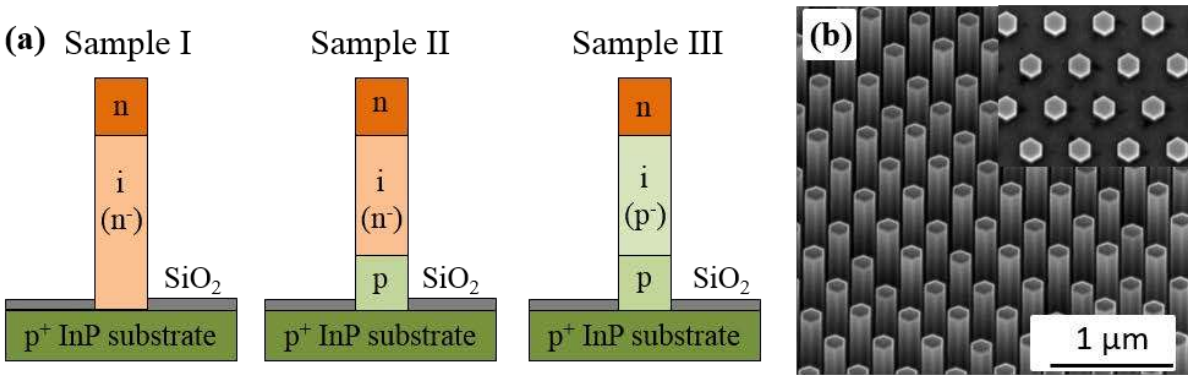

FIGURE 1. (a) Schematic of the three samples used in this study with different p-n junction designs. Due to the background impurity doping, the unintentionally doped InP i-region grown by MOVPE is normally n-type (n^-). (b) SEM image at 45° tilt view of the as-grown InP NWs. Inset shows the top view SEM image.

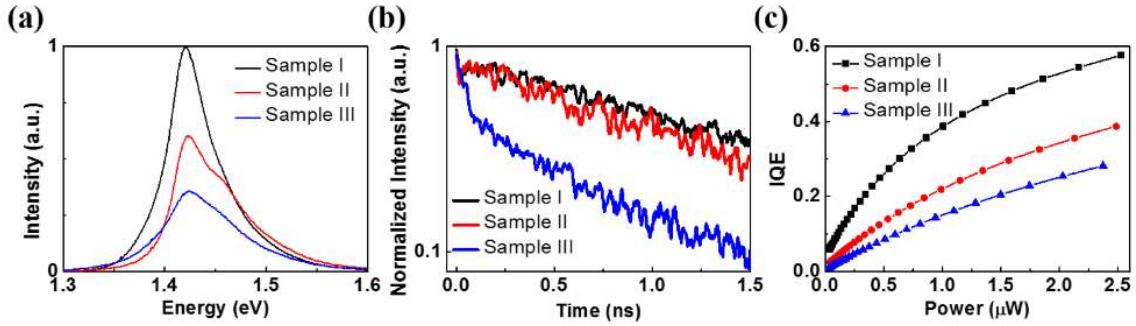

FIGURE 2. Optical properties of Samples I, II and III. (a) Typical room-temperature PL spectra of single NWs from Samples I, II and III. (b) TRPL decays measured at the peak emission wavelength of NWs from Samples I, II and III. (c) The IQE as a function of excitation power from Samples I, II and III. The curves are calculated from fitting the carrier rate equation using the method described by Fan *et al*.[24]

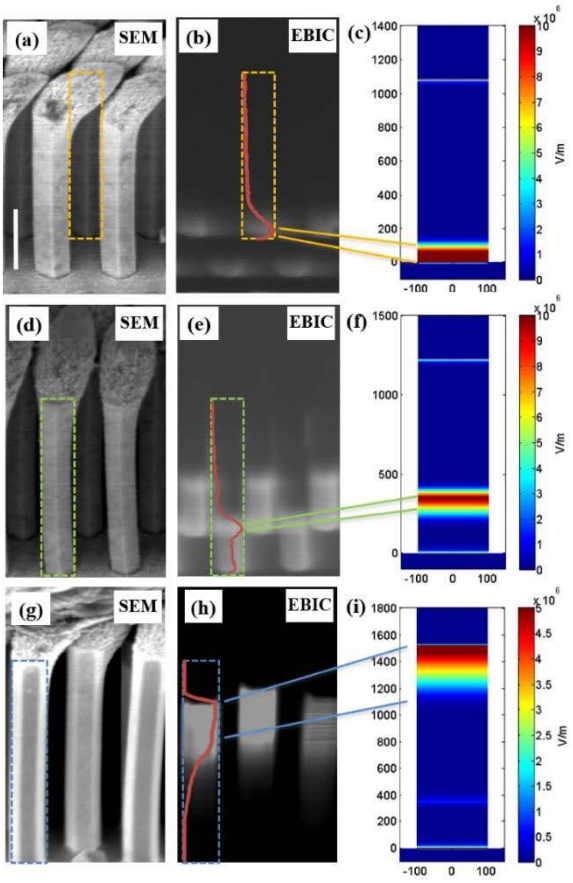

FIGURE 3. SEM, EBIC and simulation results of Samples I, II and III. (a-c), (d-f) and (g-i) present the results for Samples I, II and III, respectively. (a), (d) and (g) are SEM images at 1 kV. The ITO deposited on top of InP NW arrays using glancing angle sputter coating can be clearly observed in each image. (b), (e) and (h) are the corresponding EBIC signals of Samples I, II and III, respectively. Red curves are the relative EBIC intensity along the center of each NWs processed using ImageJ software. (c), (f) and (i) are electric field simulation results of Samples I, II and III,

respectively. The scale bar is 500 nm and all micrographs have the same magnification.

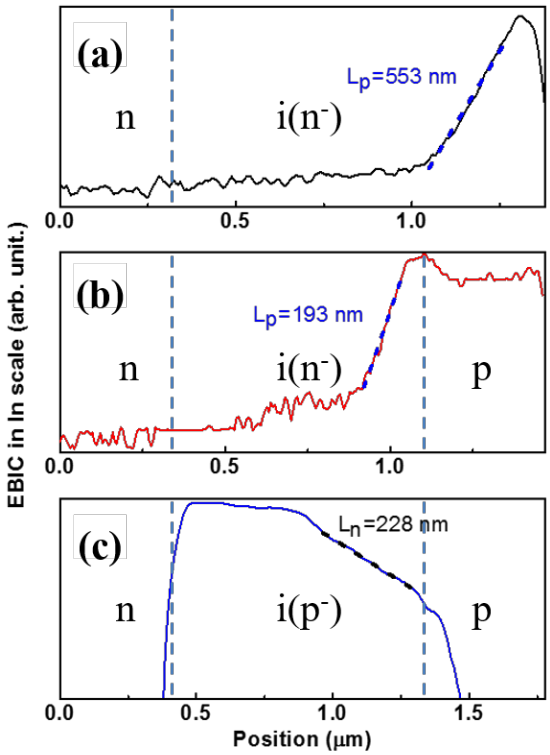

FIGURE 4. EBIC signal intensity profile along the center of the wire for (a) Sample I, (b) Sample II and (c) Sample III, respectively. The carrier diffusion lengths are extracted by analyzing the exponential decay of the current signal. The position at 0 μm represents the top of the NWs.

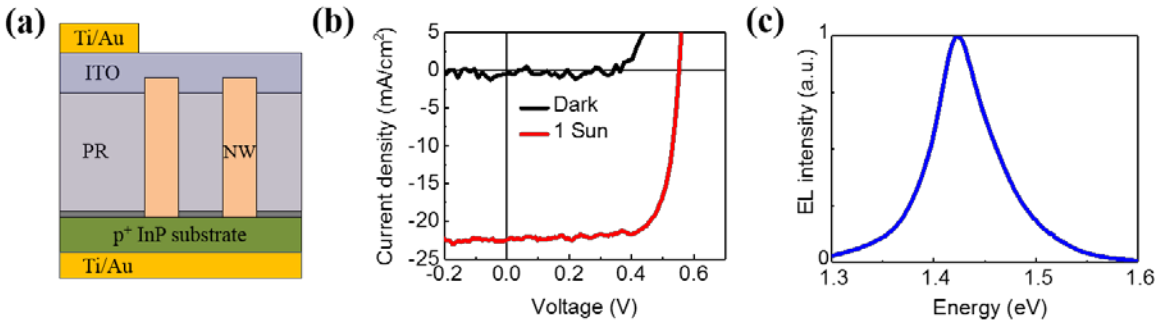

FIGURE 5. (a) Schematic layout of the fabricated solar cell device. Photoresist (PR) is used as the planarization layer, ITO as the transparent top contact and Ti/Au as the bottom contact layer. Ti/Au is deposited on top of ITO in a small area (outside the NW array) to allow external connection for electrical measurements. (b) The J-V characteristics under dark (black curve) and 1 Sun @ AM1.5G illumination (red curve) conditions measured from Sample III device. (c) Room-temperature EL spectrum of the solar cell device.

Table of contents entries

Axial p-n junction design and characterization for InP nanowire array solar cells

Qian Gao, Ziyuan Li, Li Li, Kaushal Vora, Zhe Li, Ahmed Alabadla, Fan Wang, Yanan Guo, Kun Peng, Yesaya C. Wenas, Sudha Mokkapati, Fouad Karouta, Hark Hoe Tan, Chennupati Jagadish, and Lan Fu*

III-V compound semiconductor nanowires are promising for development of high-efficiency, low-cost, flexible solar cells. Different axial p-n junction nanowire array solar cell structures are designed and investigated by nanoscale material/device characterization and simulation techniques. It is demonstrated that by varying the junction design of the nanowire solar cell, the junction position and width can be tailored towards optimal device performance.

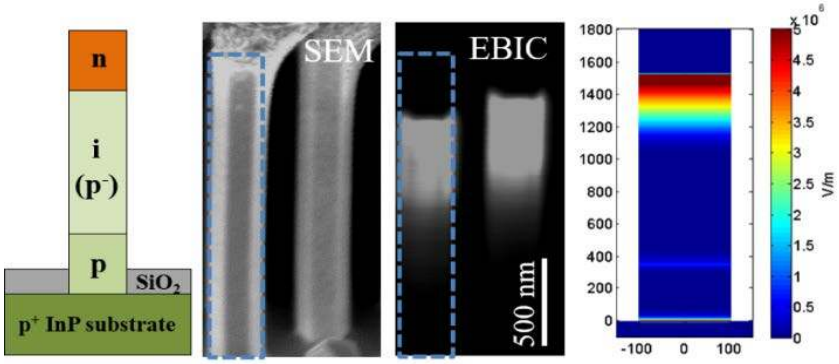

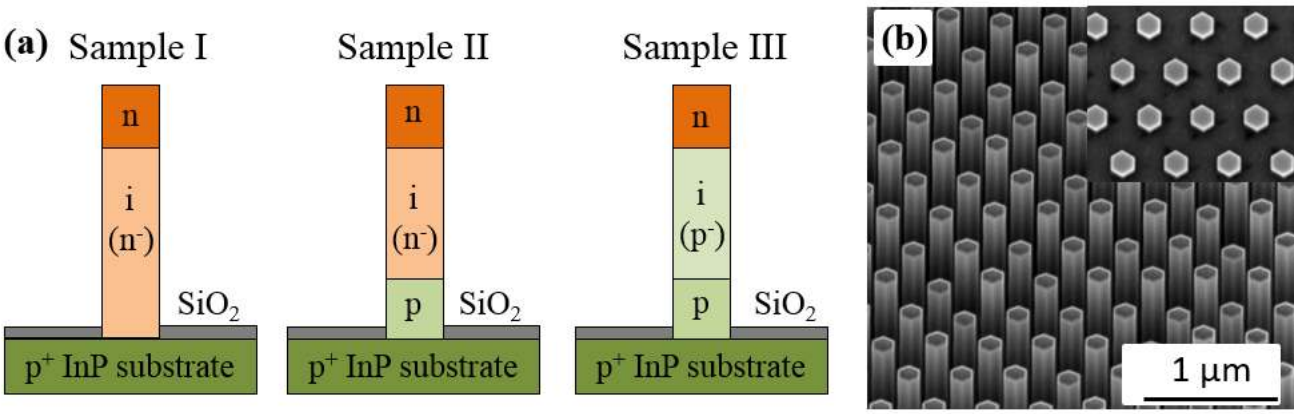

PIP_3083_F1.tif

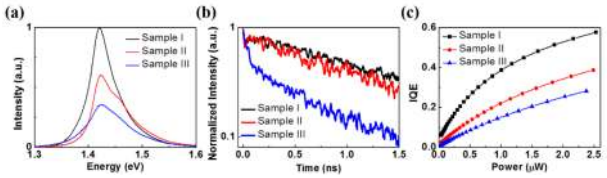

PIP_3083_F2.tif

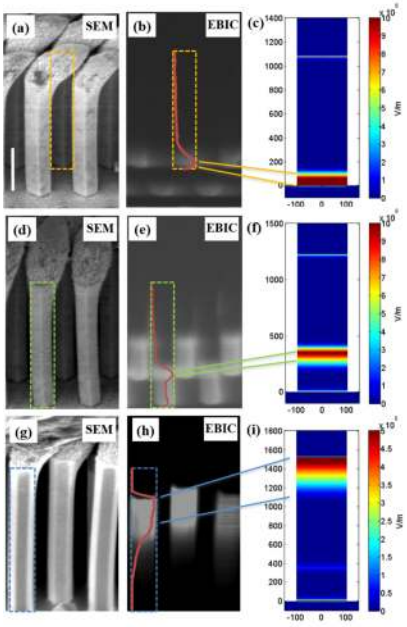

PIP_3083_F3.tif

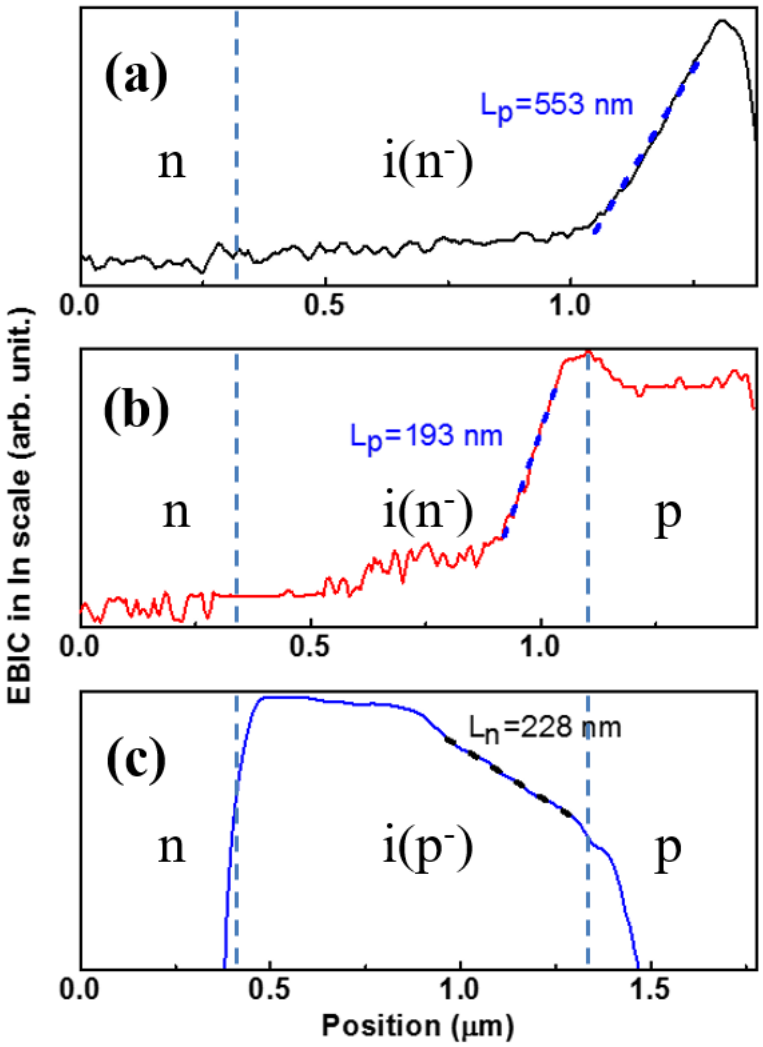

PIP_3083_F4.tif

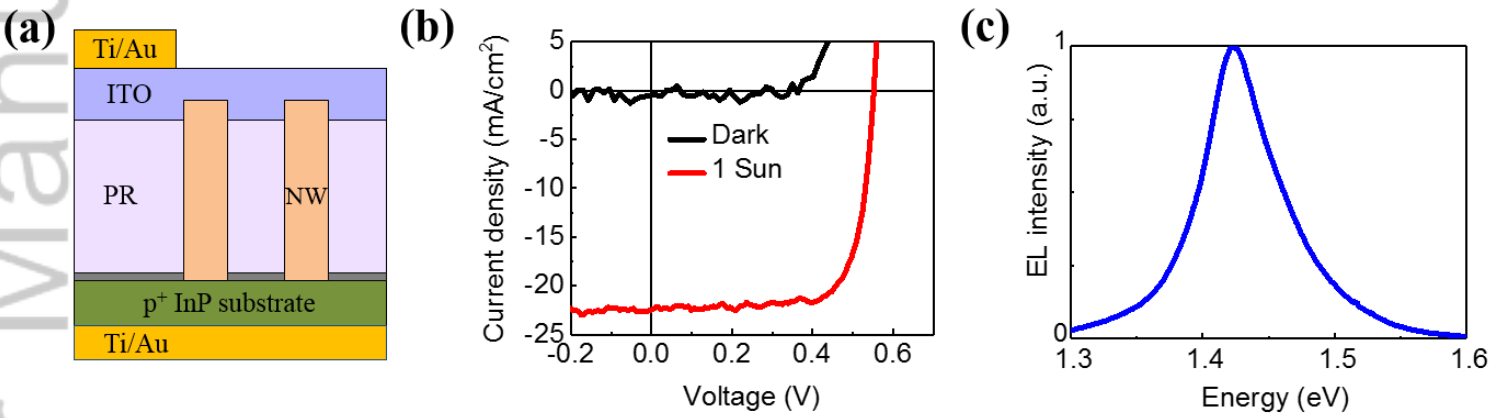

PIP_3083_F5.tif

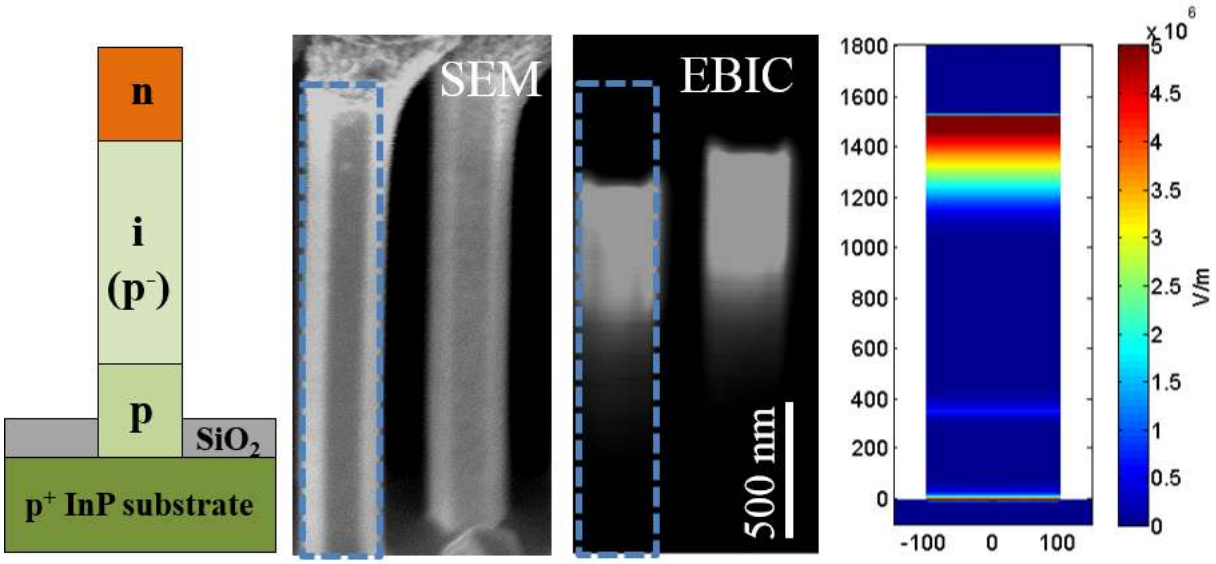

PIP_3083_GTOC.tif